SIAM J. SCI. COMPUT.
Vol. 31, No. 1, pp. 273–302

DYNAMICS OF A CLOSED ROD WITH TWIST AND BEND IN FLUID*

SOOKKYUNG LIM†, ANCA FERENT‡, X. SHELDON WANG§, AND CHARLES S. PESKIN‡

Abstract. We investigate the instability and subsequent dynamics of a closed rod with twist and bend in a viscous, incompressible fluid. A new version of the immersed boundary (IB) method is used in which the immersed boundary applies torque as well as force to the surrounding fluid and in which the equations of motion of the immersed boundary involve the local angular velocity as well as the local linear velocity of the fluid. An important feature of the IB method in this context is that self-crossing of the rod is automatically avoided because the rod moves in a continuous (interpolated) velocity field. A rod with a uniformly distributed twist that has been slightly perturbed away from its circular equilibrium configuration is used as an initial condition, with the fluid initially at rest. If the twist in the rod is sufficiently small, the rod simply returns to its circular equilibrium configuration, but for larger twists that equilibrium configuration becomes unstable, and the rod undergoes large excursions before relaxing to a stable coiled configuration.

Key words. equilibria, supercoiling, immersed boundary method, Kirchhoff theory

AMS subject classifications. 65-04, 65M06, 76D05, 76M20

DOI. 10.1137/070699780

1. Introduction.

Supercoiling (writhing) dynamics are observed, for example, in the structural deformation of DNA [29, 30, 31] and in the growth of filaments of the bacterium *Bacillus subtilis* [22, 23, 24]. The overwound or underwound double helix of DNA occurs in DNA transcription, DNA replication, and formation of DNA loops in protein-DNA interactions, which are essential in biological processes. The rod-shaped bacterium *B. subtilis* elongates and then divides and separates as it grows, but some cells fail to separate, and this results in supercoiling of the chain of attached bacteria.

Kirchhoff's rod model has been employed to study these biomechanical phenomena. The Kirchhoff model describes the rod as a three-dimensional space curve accompanied by an orthonormal triad (material frame, not to be confused with the Frenet frame of differential geometry) at each point that keeps track of the local orientation of the material. The theory of Kirchhoff for a thin elastic rod [7] has been developed to find stable and unstable equilibrium configurations and to analyze the dynamics of the supercoiling instability, with or without taking into account self-contact forces. The study of a bent and twisted rod can be performed either in the absence of fluid [4, 5, 14, 15, 16, 17, 19, 29, 33] or in the presence of fluid [3, 13, 32] in which the rod is immersed.

*Received by the editors August 3, 2007; accepted for publication (in revised form) May 5, 2008; published electronically October 16, 2008. This work was supported in part by the National Science Foundation under agreement 0112050 at the Mathematical Biosciences Institute of Ohio State University, where the first author was a postdoctoral fellow.

http://www.siam.org/journals/sisc/31-1/69978.html

†Corresponding author. Mathematical Biosciences Institute, Ohio State University, 231 West 18th Ave., Columbus, OH 43210. Current address: University of Cincinnati, 839 Old Chem, Cincinnati, OH 45221 (limsk@math.uc.edu).

‡Courant Institute of Mathematical Sciences, New York University, 251 Mercer St., New York, NY 10012 (ferent@cims.nyu.edu, peskin@cims.nyu.edu). The second author received postdoctoral support from INRIA (France).

§Department of Mathematical Sciences, New Jersey Institute of Technology, 323 Martin Luther King, Jr., Blvd., Newark, NJ 07102 (xwang@njit.edu).

In this paper we focus on the supercoiling instability of a circular rod (i.e., a ring) in a viscous fluid. We consider an elastic circular rod with an initially uniform twist that adds up to an integer number of full turns so that the triad configuration of our material frame is smoothly periodic. (The restriction to an integer number of turns is not a fundamental one in the case of a rod with circular cross section, but we make that restriction anyway to avoid dealing with a material frame described by a multivalued triad.) The rod is assumed to be isotropic, homogeneous, and embedded in a viscous incompressible fluid. We represent the rod as a space curve, and we keep track of the orientation of an orthonormal triad (material frame) at each point of the space curve so that we may know how much the rod twists or bends. The triad rotates at the local angular velocity of the fluid and applies torque locally to the fluid.

In the standard Kirchhoff rod model, the material frame is not independent of the space curve that defines the centerline of the rod. In particular, one of the vectors of the triad is constrained to be tangent to the space curve. Another constraint that is normally imposed on the Kirchhoff rod model is that of inextensibility: the rod can bend and twist, but it cannot stretch. Because of the no-slip condition at the boundary of a viscous fluid, these constraints imply rather complicated boundary conditions in a fluid in which the rod is immersed. In particular, inextensibility requires $\boldsymbol{\tau}\cdot(\boldsymbol{\tau}\cdot\nabla\mathbf{u}) = 0$, where $\boldsymbol{\tau}$ is the unit tangent to the rod and $\mathbf{u}$ is the velocity field of the fluid, and keeping the triad aligned with the rod requires $(\nabla\times\mathbf{u})\times\boldsymbol{\tau} = \boldsymbol{\tau}\cdot\nabla\mathbf{u}$. These conditions on the fluid velocity field need to be imposed along the space curve that defines the position of the rod. In this paper, however, we avoid these constraints on the fluid velocity by allowing the rod to stretch and also by allowing the orientation of the triad to deviate from alignment with the direction of the space curve. Instead of imposing the above constraints exactly, we postulate an elastic energy function which tends to maintain them. Thus, our rod is allowed to stretch slightly, and our triad is allowed to deviate slightly from the alignment with the tangent direction to the rod.

The immersed boundary (IB) method [27] is used to analyze the dynamics and the instability of a closed circular rod with twist and bend in fluid. The IB method was created to study fluid dynamics of heart valves [25, 26, 28] and has been applied to many problems mostly in biofluids [8, 9, 11, 12, 18, 20, 34]. The present work requires a significant generalization of the IB method, and an important aim of the paper is to introduce this generalization. (For a preliminary presentation, see [10].) In the original IB method the immersed boundary moves at the local fluid velocity and applies force locally to the fluid. Here we must keep track not only of the position of each point of the immersed boundary, but also of the local orientation of the immersed boundary, as expressed by the local material frame, or triad, that is carried along with each material point of the immersed elastic rod. The equation of motion of each such triad is that it rotates at the local angular velocity of the fluid. It follows from this (by the duality of torque and angular velocity, which is analogous to that of force and linear velocity) that the influence of the immersed boundary on the fluid must be expressed in terms of torque as well as force. The generalized IB method discussed herein is therefore characterized by two features: (1) that the local angular velocity of the fluid at the immersed boundary is evaluated along with the local linear velocity of the fluid, and (2) that the immersed boundary applies torque as well as force to the surrounding fluid. We show herein how to do this in a mathematically consistent way, such that the discretized power (which involves all four of the variables force, linear velocity, torque, and angular velocity) applied by the immersed boundary to the fluid has the same value whether it is computed in Lagrangian or in Eulerian variables. A limitation of the proposed method, at least in its current form, is that it is only first

order accurate. This is shown by an empirical convergence study.

One of the main issues in modeling supercoiling phenomena is *self-contact*, in which one point of the rod touches another point on the rod. It is usually necessary in this situation to prescribe self-contact forces which do not allow the rod to pass through itself. However, the generalized IB method combined with the unconstrained Kirchhoff rod theory which will be described in this paper has the ability to prevent self-crossing *without* the prescription of special conditions. In the present context the rod does not go through itself because of the continuity of the interpolated fluid velocity field (see section 3), which means there is no need to add artificial conditions that prevent self-crossing. This is rigorously true in the continuous IB formulation of the problem and remains true in practice if discretization parameters are appropriately chosen.

In section 2, we describe the balance equations of force and moment, and we discuss the equilibrium configurations of a closed circular rod in a horizontal plane. A sinusoidal perturbation is introduced to study the instability of elastic rods. The sinusoidally perturbed rod, in a fluid at rest, will be used as an initial condition in our simulations. The IB method is both a mathematical formulation and a numerical method that will describe the interaction between a bent, twisted rod and the fluid in which it is immersed. The mathematical formulation will be stated in section 3 followed by the description of the numerical scheme in section 4. In section 5, numerical results concerning equilibria of a closed rod will be discussed. We present various shapes of supercoiled equilibrium configurations depending on an intrinsic twist, perturbation parameter, and the ratio of the bend and twist moduli. The paper concludes in section 6. An appendix is provided which describes the unconstrained Kirchhoff rod model that is used in this work.

2. Equilibrium configuration of a twisted ring. Because of the nonstandard features of our Kirchhoff rod model, as described above, we need to derive the equilibrium configuration of a twisted circular rod. The configuration that we find will be close to the standard one (see [21], but see comment below) and will approach the standard equilibrium configuration as the stretch modulus b_3 and the shear force constants b_1 and b_2 all approach infinity. Another purpose of this section is to introduce our rod model, before putting it in fluid, and to state its governing equations.

An elastic rod can be represented by a space curve $\mathbf{X}(s)$ together with an orthonormal director basis $\{\mathbf{D}^1(s), \mathbf{D}^2(s), \mathbf{D}^3(s)\}$, where s is a Lagrangian parameter (not necessarily arclength) along the rod. It is assumed that the rod has a circular cross section with constant radius. The triad $\{\mathbf{D}^1(s), \mathbf{D}^2(s), \mathbf{D}^3(s)\}$ is a material frame at each point of the rod subject to the constraints $\mathbf{D}^i \cdot \mathbf{D}^j = \delta_{ij}, i, j = 1, 2, 3$. In the standard Kirchhoff rod model, one of the triad vectors (usually $\mathbf{D}^3$) is constrained to point in the direction of the tangent vector $\frac{\partial \mathbf{X}}{\partial s}$, but we do not impose this constraint here. Instead we provide forces that tend to keep $\mathbf{D}^3$ aligned with $\frac{\partial \mathbf{X}}{\partial s}$, as described below.

The force $\mathbf{F}$ and moment $\mathbf{N}$ transmitted across a section of the rod can be obtained by averaging the stresses acting across that section. Balance of momentum and angular momentum yield

$$0 = \mathbf{f} + \frac{\partial \mathbf{F}}{\partial s}, \tag{1}$$

$$0 = \mathbf{n} + \frac{\partial \mathbf{N}}{\partial s} + \frac{\partial \mathbf{X}}{\partial s} \times \mathbf{F}, \tag{2}$$

where $\mathbf{f}$ and $\mathbf{n}$ are force per unit length as measured by the parameter s and torque per unit length as measured by the parameter s applied to the rod, respectively [1, 21]. (Recall that s is not arclength in general. The variables $\mathbf{f}$ and $\mathbf{n}$ are densities with respect to the measure ds.)

The internal force and moment on the perpendicular cross section, $\mathbf{F}$, $\mathbf{N}$, and also the applied force density $\mathbf{f}$ and the torque density $\mathbf{n}$ may be expanded in the basis $\{\mathbf{D}^1, \mathbf{D}^2, \mathbf{D}^3\}$ as

$$\mathbf{F} = F^1\mathbf{D}^1 + F^2\mathbf{D}^2 + F^3\mathbf{D}^3, \tag{3}$$

$$\mathbf{N} = N^1\mathbf{D}^1 + N^2\mathbf{D}^2 + N^3\mathbf{D}^3, \tag{4}$$

$$\mathbf{f} = f^1\mathbf{D}^1 + f^2\mathbf{D}^2 + f^3\mathbf{D}^3, \tag{5}$$

$$\mathbf{n} = n^1\mathbf{D}^1 + n^2\mathbf{D}^2 + n^3\mathbf{D}^3, \tag{6}$$

and the constitutive relations of the version of the Kirchhoff rod used here are as follows:

$$N^1 = a_1\frac{\partial \mathbf{D}^2}{\partial s}\cdot\mathbf{D}^3, \quad N^2 = a_2\frac{\partial \mathbf{D}^3}{\partial s}\cdot\mathbf{D}^1, \quad N^3 = a_3\frac{\partial \mathbf{D}^1}{\partial s}\cdot\mathbf{D}^2, \tag{7}$$

$$F^1 = b_1\mathbf{D}^1\cdot\frac{\partial \mathbf{X}}{\partial s}, \quad F^2 = b_2\mathbf{D}^2\cdot\frac{\partial \mathbf{X}}{\partial s}, \quad F^3 = b_3\left(\mathbf{D}^3\cdot\frac{\partial \mathbf{X}}{\partial s} - 1\right), \tag{8}$$

where a_1 and a_2 are the bending moduli of the rod about $\mathbf{D}^1$ and $\mathbf{D}^2$, respectively, and where a_3 is the twisting modulus of the rod. These moduli are standard in the Kirchhoff rod model. Note that $a_1 = a_2$ in the case of a rod with a circular cross section and axially symmetric material properties. The constitutive equations (8) are the means by which we approximately enforce the constraints that $s =$ arclength and that $\mathbf{D}^3$ should point in the same direction as $\frac{\partial \mathbf{X}}{\partial s}$. As we show in the appendix, the above unconstrained version of the Kirchhoff rod model can be derived from a variational argument in which we postulate an elastic energy of the form

$$\begin{aligned} E = \frac{1}{2}\int \Bigg[& a_1\left(\frac{d\mathbf{D}^2}{ds}\cdot\mathbf{D}^3\right)^2 + a_2\left(\frac{d\mathbf{D}^3}{ds}\cdot\mathbf{D}^1\right)^2 + a_3\left(\frac{d\mathbf{D}^1}{ds}\cdot\mathbf{D}^2\right)^2 \\ & + b_1\left(\mathbf{D}^1\cdot\frac{d\mathbf{X}}{ds}\right)^2 + b_2\left(\mathbf{D}^2\cdot\frac{d\mathbf{X}}{ds}\right)^2 + b_3\left(\mathbf{D}^3\cdot\frac{d\mathbf{X}}{ds} - 1\right)^2\Bigg] ds. \end{aligned} \tag{9}$$

To find an equilibrium configuration of a circular rod in a horizontal plane we introduce cylindrical coordinates (r, θ, z) with unit vectors $(\mathbf{r}(\theta), \boldsymbol{\theta}(\theta), \mathbf{z})$. Recall that

$$\mathbf{r}(\theta) = (\cos\theta, \sin\theta, 0), \tag{10}$$

$$\boldsymbol{\theta}(\theta) = (-\sin\theta, \cos\theta, 0), \tag{11}$$

$$\mathbf{z} = (0, 0, 1), \tag{12}$$

and $\mathbf{r}'(\theta) = \boldsymbol{\theta}(\theta), \boldsymbol{\theta}'(\theta) = -\mathbf{r}(\theta)$. Let $s = r_0\theta, 0 \le s \le 2\pi r_0$, and then construct the configuration $\mathbf{X}(s)$ and the orthonormal triad $\{\mathbf{D}^1(s), \mathbf{D}^2(s), \mathbf{D}^3(s)\}$ as follows:

$$\mathbf{X}(s) = r_1\mathbf{r}(s/r_0), \tag{13}$$

$$\mathbf{D}^3(s) = (\cos\beta)\boldsymbol{\theta}(s/r_0) + (\sin\beta)\mathbf{z}, \tag{14}$$

$$\mathbf{E}(s) = -(\sin\beta)\boldsymbol{\theta}(s/r_0) + (\cos\beta)\mathbf{z}, \tag{15}$$

$$\mathbf{D}^1(s) = \cos(ps/r_0)\mathbf{E}(s) + \sin(ps/r_0)\mathbf{r}(s/r_0), \tag{16}$$

$$\mathbf{D}^2(s) = -\sin(ps/r_0)\mathbf{E}(s) + \cos(ps/r_0)\mathbf{r}(s/r_0), \tag{17}$$

where β is a constant (to be determined below) and p is the integer which determines the density of twist uniformly distributed along the rod. The reason we restrict p to integer values is so that the triad will be continuous at $s = 0$, which is the same point as $s = 2\pi r_0$. For an axially symmetric rod, there is no physical discontinuity if we choose noninteger p, but this case needs to be handled with a triad that is not single-valued, and we avoid that situation here. The vector $\mathbf{D}^3$ lies on the tangent plane spanned with azimuthal and axial components but slightly tilted away from the tangent vector to the rod $\mathbf{X}(s)$. The vector $\mathbf{E}(s)$ is a useful reference vector orthogonal to $\mathbf{D}^3$ within the plane spanned by $\boldsymbol{\theta}$ and $\mathbf{z}$.

For simplicity, we consider an isotropic rod in this paper, i.e., $a_1 = a_2 \equiv a$, and we also assume that $b_1 = b_2 = b_3 \equiv b$.

By substituting the above formulae for $\mathbf{X}(s)$, $\mathbf{D}^1(s)$, $\mathbf{D}^2(s)$, and $\mathbf{D}^3(s)$ into the constitutive relations (7) and (8), we can find formulae for $\mathbf{F}(s)$ and $\mathbf{N}(s)$. These results in turn can be substituted into the equilibrium equations (1) and (2) in the absence of any applied forces or moments, i.e., with $\mathbf{f}(s)$ and $\mathbf{n}(s)$ both equal to zero. It turns out that the two equilibrium equations are satisfied if and only if

$$r_1 = r_0\cos\beta, \tag{18}$$

$$\sin\beta = -\frac{a_3 p}{br_0^2 + a_3 - a}. \tag{19}$$

For large b, β is a small angle, which implies that the triad constructed above is nearly aligned with the rod, and also that r_1 is just slightly smaller than the unstressed radius r_0. In the limit $b \to \infty$, we recover the standard circular equilibrium of a twisted Kirchhoff ring. (See Figure 1.)

The behavior of $\mathbf{F}(s)$ in the solution constructed above, and indeed in the standard circular equilibrium of a twisted Kirchhoff ring, is perhaps somewhat unexpected, and we comment on it here. The first equilibrium equation states that $\mathbf{F}(s)$ has to be constant, independent of s, and one might then be tempted to conclude that $\mathbf{F}$ has to be zero, by symmetry. This conclusion is incorrect. What we actually find is that

$$\mathbf{F} = -b(\sin\beta)\mathbf{z} = \frac{ba_3 p}{br_0^2 + a_3 - a}\mathbf{z}. \tag{20}$$

As $b \to \infty$, $\mathbf{F} \to (a_3 p/r_0^2)\mathbf{z}$. Thus, the constant vector $\mathbf{F}$, which represents the force transmitted across a section of the rod, points normal to the horizontal plane in which the rod lies. This seems strange (what determines whether the force is up

(a) $p = 2$ (b) $p = 5$

FIG. 1. *Examples of equilibrium configurations of twisted rings with only* $\mathbf{D}^1$ *shown. The parameter* p *is the number of twists.*

or down?) until we recall that $\mathbf{F}(s_0)$ is the force applied by the part of the rod for which s is slightly greater than s_0 to the part of the rod for which s is slightly less than s_0 across the section of the rod at $s = s_0$. A force of the same magnitude but pointing in the opposite direction is applied by the part of the rod with s slightly less than s_0 to the part with s slightly greater than s_0, so it is merely the direction in which we choose to traverse the rod that determines whether $\mathbf{F}$ points up or down. Nevertheless, this result is sufficiently peculiar that it led Love [21, p. 417] to state erroneously, "and the shearing force at any section is directed towards the center of the circle." This sounds reasonable, considering the symmetry of the problem, but it clearly cannot be correct, as it violates the equilibrium condition that $\mathbf{F}$ must be constant!

In computer simulations, however, we use a perturbed configuration as an initial configuration to see whether the equilibrium configuration constructed above is stable or unstable. A sinusoidal perturbation can be obtained by making the following substitutions in the formulae for $\mathbf{D}^1$ and $\mathbf{D}^2$:

$$\sin\left(\frac{ps}{r_0}\right) \to \sin\left(\frac{ps}{r_0} + \epsilon \sin\frac{s}{r_0}\right), \tag{21}$$

$$\cos\left(\frac{ps}{r_0}\right) \to \cos\left(\frac{ps}{r_0} + \epsilon \sin\frac{s}{r_0}\right), \tag{22}$$

where ϵ is a perturbation parameter (see Figure 2).

3. Mathematical formulation. The equations of motion for a bent, twisted rod immersed in a viscous incompressible fluid are stated in this section. They involve both Eulerian and Lagrangian variables. The Eulerian variables are used to describe the fluid, and the Lagrangian variables are used to describe the immersed rod. These two types of variables may be interconverted by means of integral transformations that involve a smoothed version of the three-dimensional Dirac delta function, as will be seen below.

We consider a viscous, incompressible fluid governed by the Navier–Stokes equations, and a closed bent and twisted rod immersed in that fluid. The immersed rod is represented as a one-dimensional closed curve with an associated orthonormal triad at each point of the curve. In describing the immersed rod, we use the same notation as in the previous section. There, $\mathbf{f}(s)ds$ was the force applied by some unspecified external agent to the arc ds of the rod. Here, that external agent is the fluid, and

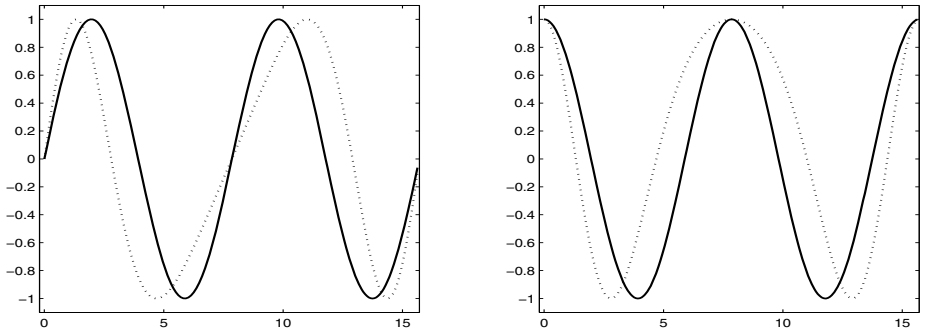

(a) (b)

FIG. 2. *Sinusoidal perturbation in* $\{\mathbf{D}^1, \mathbf{D}^2\}$ *when* $p = 2$, $\epsilon = 1$. (a) *sine function (solid) and its perturbation (dotted) (see* (21)*).* (b) *cosine function (solid) and its perturbation (dotted) (see* (22)*).*

therefore (according to Newton) $-\mathbf{f}(s)ds$ is the force applied by the arc ds of the rod to the fluid. Similarly, $-\mathbf{n}(s)ds$ is the torque applied by the arc ds of the rod to the fluid.

The interaction of a viscous incompressible fluid with a thin elastic rod presents the following conceptual difficulty: on the one hand, it seems natural to represent the rod as a space curve (with its associated triad) as in the previous section. On the other hand, it is impossible to describe the interaction of a space curve with a three-dimensional fluid, since the application of a finite force per unit length along a curve in such a fluid results in a velocity field that is infinite on that curve. (This is in sharp contrast to the case of a surface on which the application of finite force per unit area results in a finite velocity everywhere, including on the surface itself. The difference between these two cases is that the surface is codimension 1, whereas the curve is codimension 2.) Thus, we must somehow assign a cross-sectional radius to the space curve that represents the bent, twisted rod. In the present work, this will be done by replacing the Dirac delta function that appears in the interaction equations of the IB method by a smoothed approximation to the delta function that we denote δ_c, where the subscript c denotes the order of magnitude of the support of the smoothed delta function. The specific form of δ_c will be specified below. In typical applications of the IB method, the mathematical formulation of the problem involves the true Dirac delta function, and a smoothed approximation to the delta function makes its appearance only at the level of the spatially discretized equations. Here, we need the smoothed approximation from the outset for our formulation to make sense, and it is important to keep in mind that c is a physical parameter of the problem, as it determines the effective radius of the rod. In practice, we choose the meshwidth h of the lattice on which the Navier–Stokes equations are solved equal to c in most of our simulations, but we also set it equal to $c/2$ for comparison, in order to check the convergence of our scheme. This convergence test is described at the end of section 5.

Related to the above is the conceptual issue of the mass of the rod. We assume in the present work that the rod is neutrally buoyant, i.e., that its mass is equal to the mass of the fluid displaced. In an IB computation, however, the fluid is not displaced; it permeates the volume of radius $O(c)$ that surrounds the space curve that

represents the rod. Thus, in our computational method, the fluid supplies the mass that is physically attributable to the rod, and the consistent way to model the space curve (with its associated triad) that represents the elasticity of the rod is as though it were massless. Since a massless structure is always at equilibrium, we may use unchanged the force balance equations of the previous section to describe the elastic component of our model system.

The coupled system of equations of the rod and the fluid is as follows:

$$\rho\left(\frac{\partial \mathbf{u}}{\partial t}+\mathbf{u}\cdot\nabla\mathbf{u}\right)=-\nabla p+\mu\nabla^2\mathbf{u}+\mathbf{f}^b, \tag{23}$$

$$\nabla\cdot\mathbf{u}=0, \tag{24}$$

$$0=\mathbf{f}+\frac{\partial \mathbf{F}}{\partial s}, \tag{25}$$

$$0=\mathbf{n}+\frac{\partial \mathbf{N}}{\partial s}+\frac{\partial \mathbf{X}}{\partial s}\times\mathbf{F}, \tag{26}$$

$$\mathbf{F}=F^1\mathbf{D}^1+F^2\mathbf{D}^2+F^3\mathbf{D}^3, \tag{27}$$

$$\mathbf{N}=N^1\mathbf{D}^1+N^2\mathbf{D}^2+N^3\mathbf{D}^3, \tag{28}$$

$$N^1=a_1\frac{\partial \mathbf{D}^2}{\partial s}\cdot\mathbf{D}^3,\quad N^2=a_2\frac{\partial \mathbf{D}^3}{\partial s}\cdot\mathbf{D}^1,\quad N^3=a_3\frac{\partial \mathbf{D}^1}{\partial s}\cdot\mathbf{D}^2, \tag{29}$$

$$F^1=b_1\mathbf{D}^1\cdot\frac{\partial \mathbf{X}}{\partial s},\quad F^2=b_2\mathbf{D}^2\cdot\frac{\partial \mathbf{X}}{\partial s},\quad F^3=b_3\left(\mathbf{D}^3\cdot\frac{\partial \mathbf{X}}{\partial s}-1\right), \tag{30}$$

$$\mathbf{f}^{\mathrm{b}}(\mathbf{x},t)=\int(-\mathbf{f}(s,t))\,\delta_c(\mathbf{x}-\mathbf{X}(s,t))ds+\frac{1}{2}\nabla\times\int(-\mathbf{n}(s,t))\delta_c(\mathbf{x}-\mathbf{X}(s,t))ds, \tag{31}$$

$$\frac{\partial \mathbf{X}(s,t)}{\partial t}=\mathbf{U}(s,t)=\int\mathbf{u}(\mathbf{x},t)\,\delta_c(\mathbf{x}-\mathbf{X}(s,t))d\mathbf{x}, \tag{32}$$

$$\mathbf{W}(s,t)=\frac{1}{2}\int(\nabla\times\mathbf{u})\delta_c(\mathbf{x}-\mathbf{X}(s,t))d\mathbf{x}, \tag{33}$$

$$\frac{\partial \mathbf{D}^i(s,t)}{\partial t}=\mathbf{W}(s,t)\times\mathbf{D}^i(s,t),\quad i=1,2,3. \tag{34}$$

Equations (23)–(24) are the incompressible Navier–Stokes equations written in Eulerian variables $(\mathbf{x},t)$, where $\mathbf{x}=(x_1,x_2,x_3)$ are fixed Cartesian coordinates and t is the time. The motion of the fluid is subject to the body force $\mathbf{f}^{\mathrm{b}}(\mathbf{x},t)$, which here represents the force per unit volume applied to the fluid by the immersed rod. The vector field $\mathbf{u}(\mathbf{x},t)$ is the fluid velocity, and $p(\mathbf{x},t)$ is the fluid pressure. The constant parameters ρ and μ are the fluid density and the fluid viscosity, respectively.

The equilibrium equations (25)–(30) of the previous section are employed to describe the force and torque of the immersed rod in terms of the space curve and its associated triad

$$\left(\mathbf{X}(s,t),\mathbf{D}^1(s,t),\mathbf{D}^2(s,t),\mathbf{D}^3(s,t)\right). \tag{35}$$

All variables in these equilibrium equations are functions of the material coordinate s (not necessarily arclength) and the time t. These are therefore Lagrangian variables. As in the previous section, $\mathbf{F}(s,t)$ and $\mathbf{N}(s,t)$ are the force and moment (couple) transmitted across the section of the rod at s. The expressions $-\mathbf{f}(s,t)ds$ and $-\mathbf{n}(s,t)ds$ are the force and torque applied by the arc ds of the rod to the fluid.

Equations (31)–(33) describe the interactions between the fluid and the rod. These interaction equations connect the Lagrangian and Eulerian variables via a three-dimensional smoothed Dirac delta function $\delta_c(\mathbf{x}) = \delta_c(x_1)\delta_c(x_2)\delta_c(x_3)$, which acts as a kernel of the integral transformations that appear in the interaction equations. The particular choice of $\delta_c(\mathbf{x})$ that we make in this work is the following:

$$\delta_c(\mathbf{x}) = \frac{1}{c^3}\phi\left(\frac{x_1}{c}\right)\phi\left(\frac{x_2}{c}\right)\phi\left(\frac{x_3}{c}\right), \tag{36}$$

where $\mathbf{x} = (x_1, x_2, x_3)$ and the function ϕ is given by

$$\phi(r) = \begin{cases} \dfrac{3 - 2|r| + \sqrt{1 + 4|r| - 4r^2}}{8} & \text{if } |r| \le 1, \\ \dfrac{5 - 2|r| - \sqrt{-7 + 12|r| - 4r^2}}{8} & \text{if } 1 \le |r| \le 2, \\ 0 & \text{if } |r| \ge 2. \end{cases}$$

The motivation for this particular construction is discussed in [28, 27]. Without going into all of the details, we note in particular that $\delta_c(\mathbf{x}-\mathbf{X})$ is a continuous function of $\mathbf{x}$ with continuous first derivatives and with support equal to a cube of edge $4c$ centered on $\mathbf{X}$. Whenever c is an integer multiple of h, the function $\delta_c(\mathbf{x} - \mathbf{X})$ satisfies two identities that are of particular importance in this work. Note in particular that these identities hold for all $\mathbf{X}$:

$$\sum_{\mathbf{j}} \delta_c(\mathbf{j}h - \mathbf{X})h^3 = 1, \tag{37}$$

$$\sum_{\mathbf{j}} (\mathbf{j}h - \mathbf{X})\delta_c(\mathbf{j}h - \mathbf{X})h^3 = 0, \tag{38}$$

where $\mathbf{j}$ is any vector with integer components and h is the meshwidth of the fluid grid that will be introduced in the next section. As mentioned above, these identities hold only if c/h is a positive integer, and we shall choose h so that this is the case. The significance of the above identities will become apparent when we prove, in the next section, that force and torque generated by the rod are correctly applied to the fluid by our numerical scheme.

In (31), the first term describes how to apply the force of the rod to the fluid and the second term describes how to apply the torque of the rod to the fluid. To understand the meaning of (31), take the dot product of both sides with an arbitrary velocity field $\mathbf{u}(\mathbf{x},t)$ and integrate by parts in the second term. (Note in particular that the overall sign of the second term does not change upon this integration by parts because the usual sign change is compensated by a change of sign involving the antisymmetry of the cross product.) The result is

$$\int \mathbf{u}(\mathbf{x},t)\cdot\mathbf{f}^{\mathrm{b}}(\mathbf{x},t)d\mathbf{x} = \int(-\mathbf{f}(s,t))\cdot\mathbf{U}(s,t)ds + \int(-\mathbf{n}(s,t))\cdot\mathbf{W}(s,t)ds, \tag{39}$$

where $\mathbf{U}(s,t)$ is the locally averaged fluid velocity defined by (32) and $\mathbf{W}(s,t)$ is the locally averaged *angular* velocity of the fluid as defined by (33). Thus we have the result that the rate at which work is done on the fluid by the immersed rod is as it should be in terms of the force and moment applied to the fluid by the rod. Since this holds for an *arbitrary* velocity field, it establishes the validity of (31). Equation (32) is the no-slip condition of a viscous fluid, which means that the rod moves at the local fluid velocity. Here, the local fluid velocity is averaged in a manner determined by the smoothed Dirac delta function. Equation (33) states that angular velocity $\mathbf{W}(s,t)$ of the triad associated with the point s of the rod can be obtained as a local average of the angular velocity of the fluid, $\frac{1}{2}(\nabla \times \mathbf{u})$. Again, the smoothed delta function is used to determine the appropriate weighted average of the local fluid velocity.

We keep track of the orientation of the triad at each point of the rod by (34). The triad rotates at the local angular velocity of the fluid and applies torque locally to the fluid.

4. Numerical method. In this section, we describe the numerical IB method that we use to solve the equations of motion (23)–(34) as formulated in the preceding section.

The spatial discretization of the Eulerian (fluid) variables is different from that of the Lagrangian (rod) variables. For the fluid variables such as $\mathbf{u}$, p, and $\mathbf{f}^{\mathrm{b}}$, we use a fixed cubic lattice of meshwidth h. This lattice, denoted g_h, is the set of points $g_h = \{\mathbf{x} : \mathbf{x} = \mathbf{j}h\}$, where $\mathbf{j} = (j_1, j_2, j_3) \in \mathbb{Z}^3$, i.e., a vector with integer components. Although our discretization makes sense on an infinite grid, in practice we use a lattice that is periodic in all three space directions. Thus $0 \le j_i \le N-1$ for $i = 1, 2, 3$, and it is understood that arithmetic involving any of the j_i is to be done modulo N. The periodicity facilitates the use of the discrete Fourier transform and is less disruptive than other boundary conditions one might consider. In particular, a periodic domain (3-torus) is translation invariant, and all grid points are equivalent when periodic boundary conditions are used.

Spatial discretization of the immersed rod is accomplished by first introducing a fixed uniform interval $\triangle s$ of the Lagrangian variable s of the rod, and then setting $s_k = k\triangle s$, for $k = 0, 1, \ldots, l-1$, where $l\triangle s$ is the unstressed length of the rod, and it is understood that all arithmetic on k is to be done modulo l, since the rod is in fact closed. For some variables, we shall consider half-integer as well as integer values of the index k. The Lagrangian variables $\mathbf{X}$, $\mathbf{D}^1$, $\mathbf{D}^2$, $\mathbf{D}^3$, $\mathbf{f}$, and $\mathbf{n}$ will all be defined at points s_k for integer values of k, and for such variables we shall use the notation $\mathbf{X}_k = \mathbf{X}(k\triangle s)$, etc. We shall need, however, to define auxiliary $\mathbf{D}^i$ at s_k for half-integer values of k, and the variables $\mathbf{F}$ and $\mathbf{N}$ will also be defined at s_k for half-integer values of k. For such variables, we shall write $\mathbf{D}^i_{k+\frac{1}{2}}$, etc., where k is again restricted to integer values.

Let the superscript n be the time-step index, so that $\mathbf{u}^n$ denotes the fluid velocity field at time $t = n\triangle t$, where $\triangle t$ is time-step duration, and similarly for all other variables. We shall describe here the step from time level n to $n+1$. To avoid cluttering the notation, however, we omit the time index in any equation where all of the variables are to be evaluated at time level n, i.e., at the beginning of the time step. This includes all of the equations involving the elasticity of the rod, which will be discussed first. The time index will make its appearance when we come to the fluid equations and will continue to appear in the equations for updating the configuration of the rod.

The first thing that needs to be done in each time step is to compute the auxiliary

triad at the point $s_{k+\frac{1}{2}}$ from the triads at s_k and s_{k+1}, where k is any integer. Intuitively, this is an interpolation process, but we cannot use anything like linear interpolation, since the result would not be an orthonormal triad. Therefore, we proceed as follows.

A rotation (orthogonal matrix) which maps from the triad $\mathbf{D}_k^\alpha$ to the triad $\mathbf{D}_{k+1}^\alpha$ ($\alpha = 1, 2, 3$) is uniquely defined by

$$A = \sum_{\alpha=1}^{3} \mathbf{D}_{k+1}^\alpha (\mathbf{D}_k^\alpha)^T, \tag{40}$$

that is,

$$A = (a_{ij}) = \sum_{\alpha=1}^{3} (\mathbf{D}_{k+1}^\alpha)_i (\mathbf{D}_k^\alpha)_j, \tag{41}$$

where ^{T} stands for the transpose of a matrix and $i, j = 1, 2, 3$; $k = 0, \ldots, l-1$.

This matrix A can be described as a rotation about a certain axis through a certain angle. To remove the ambiguity about the angle, we choose the one with smallest magnitude, which is also the one lying in the interval $(-\pi, \pi]$.

In order to find an orthonormal triad $\{\mathbf{D}_{k+\frac{1}{2}}^1, \mathbf{D}_{k+\frac{1}{2}}^2, \mathbf{D}_{k+\frac{1}{2}}^3\}$ for the point $s_{k+\frac{1}{2}}$ we can take the principal square root of the matrix A, which is a rotation about that same axis by half the angle (and make sure that half the angle should be in the interval $(-\pi/2, \pi/2]$), and apply this rotation to each vector of the triad at s_k; i.e.,

$$\mathbf{D}_{k+\frac{1}{2}}^i = \sqrt{A}\mathbf{D}_k^i, \tag{42}$$

where $i = 1, 2, 3$. This will give the desired triad at $s_{k+\frac{1}{2}}$.

The next step is to evaluate the force $\mathbf{F}_{k+\frac{1}{2}}$ and the couple or moment $\mathbf{N}_{k+\frac{1}{2}}$ that are transmitted across the section of the rod at $s_{k+\frac{1}{2}}$. The computations are as follows. First evaluate the components

$$F_{k+\frac{1}{2}}^1 = b_1 \mathbf{D}_{k+\frac{1}{2}}^1 \cdot \frac{\mathbf{X}_{k+1} - \mathbf{X}_k}{\triangle s}, \tag{43}$$

$$F_{k+\frac{1}{2}}^2 = b_2 \mathbf{D}_{k+\frac{1}{2}}^2 \cdot \frac{\mathbf{X}_{k+1} - \mathbf{X}_k}{\triangle s}, \tag{44}$$

$$F_{k+\frac{1}{2}}^3 = b_3 \left(\mathbf{D}_{k+\frac{1}{2}}^3 \cdot \frac{\mathbf{X}_{k+1} - \mathbf{X}_k}{\triangle s} - 1 \right), \tag{45}$$

$$N_{k+\frac{1}{2}}^1 = a_1 \frac{\mathbf{D}_{k+1}^2 - \mathbf{D}_k^2}{\triangle s} \cdot \mathbf{D}_{k+\frac{1}{2}}^3, \tag{46}$$

$$N_{k+\frac{1}{2}}^2 = a_2 \frac{\mathbf{D}_{k+1}^3 - \mathbf{D}_k^3}{\triangle s} \cdot \mathbf{D}_{k+\frac{1}{2}}^1, \tag{47}$$

$$N_{k+\frac{1}{2}}^3 = a_3 \frac{\mathbf{D}_{k+1}^1 - \mathbf{D}_k^1}{\triangle s} \cdot \mathbf{D}_{k+\frac{1}{2}}^2, \tag{48}$$

which are discretizations of (29)–(30), and then assemble the vectors

$$\mathbf{F}_{k+\frac{1}{2}} = F_{k+\frac{1}{2}}^1 \mathbf{D}_{k+\frac{1}{2}}^1 + F_{k+\frac{1}{2}}^2 \mathbf{D}_{k+\frac{1}{2}}^2 + F_{k+\frac{1}{2}}^3 \mathbf{D}_{k+\frac{1}{2}}^3, \tag{49}$$

$$\mathbf{N}_{k+\frac{1}{2}} = N_{k+\frac{1}{2}}^1 \mathbf{D}_{k+\frac{1}{2}}^1 + N_{k+\frac{1}{2}}^2 \mathbf{D}_{k+\frac{1}{2}}^2 + N_{k+\frac{1}{2}}^3 \mathbf{D}_{k+\frac{1}{2}}^3. \tag{50}$$

What this last step means operationally is to evaluate the *Cartesian* components of these vectors. This is very important for what follows, since we want to compare these vectors at different locations (see below), and this cannot be done merely by comparing their components in the basis given by the moving triad.

With $\mathbf{F}_{k+\frac{1}{2}}$ and $\mathbf{N}_{k+\frac{1}{2}}$ known for all k, we can proceed to the computation of $-\mathbf{f}_k$ and $-\mathbf{n}_k$ by the following discretization of (25)–(26). These quantities, multiplied in each case by ds, give the force and torque applied to the fluid by the segment of the rod corresponding to the interval ds centered on s_k:

$$-\mathbf{f}_k = \frac{\mathbf{F}_{k+\frac{1}{2}} - \mathbf{F}_{k-\frac{1}{2}}}{\triangle s}, \tag{51}$$

$$-\mathbf{n}_k = \frac{\mathbf{N}_{k+\frac{1}{2}} - \mathbf{N}_{k-\frac{1}{2}}}{\triangle s} + \frac{1}{2}\left(\frac{\mathbf{X}_{k+1} - \mathbf{X}_k}{\triangle s} \times \mathbf{F}_{k+\frac{1}{2}} + \frac{\mathbf{X}_k - \mathbf{X}_{k-1}}{\triangle s} \times \mathbf{F}_{k-\frac{1}{2}}\right). \tag{52}$$

This completes the purely Lagrangian part of the computation during any one time step.

The force and torque generated by the elasticity of the rod can now be applied to the fluid by creating the body force $\mathbf{f}^{\mathrm{b}}$ on the fluid grid defined as follows:

$$\mathbf{f}^{\mathrm{b}}(\mathbf{x}) = \sum_k (-\mathbf{f}_k)\,\delta_c(\mathbf{x} - \mathbf{X}_k)\triangle s + \frac{1}{2}\mathbf{G}^0 \times \left(\sum_k (-\mathbf{n}_k)\,\delta_c(\mathbf{x} - \mathbf{X}_k)\triangle s\right), \tag{53}$$

where $\mathbf{x} \in g_h$ and δ_c has been defined in the preceding section. Recall in particular the restriction that c/h must be a positive integer.

Here, and throughout the paper, $\mathbf{G}^0$ denotes the central difference approximation to ∇ defined on the Eulerian grid g_h by $\mathbf{G}^0 = (G_1^0, G_2^0, G_3^0)$, where G_α^0 is the standard central difference operator in the spatial direction $\alpha = 1, 2, 3$ defined by

$$\left(G_\alpha^0 \psi\right)(\mathbf{x}) = \frac{\psi(\mathbf{x} + h\mathbf{e}^\alpha) - \psi(\mathbf{x} - h\mathbf{e}^\alpha)}{2h}, \tag{54}$$

where $\{\mathbf{e}^1, \mathbf{e}^2, \mathbf{e}^3\}$ is a fixed orthonormal basis that specifies the orientation of the Cartesian lattice on which the Eulerian variables of our fluid mechanics computation are defined. In the following we shall also make use of the forward and backward difference operators in each of the three spatial directions $\alpha = 1, 2, 3$. These are defined by

$$\left(G_\alpha^+ \psi\right)(\mathbf{x}) = \frac{\psi(\mathbf{x} + h\mathbf{e}^\alpha) - \psi(\mathbf{x})}{h}, \tag{55}$$

$$\left(G_\alpha^- \psi\right)(\mathbf{x}) = \frac{\psi(\mathbf{x}) - \psi(\mathbf{x} - h\mathbf{e}^\alpha)}{h}. \tag{56}$$

Up to this point, all quantities have been defined at time level n, i.e., at the beginning of the time step, and the superscript n indicating the time level has been omitted. Here, we begin to describe the computation of variables defined at time level $n+1$ from those at time level n, so we include the superscript that indicates the time level from now on.

With $\mathbf{u}^n$ and $(\mathbf{f}^{\mathrm{b}})^n$ known, we solve the discretized Navier–Stokes equations for the unknowns $(\mathbf{u}^{n+1}, p^{n+1})$:

$$\rho\left(\frac{\mathbf{u}^{n+1}-\mathbf{u}^n}{\triangle t}+\sum_{\alpha=1}^{3}u_\alpha^n G_\alpha^{\pm}\mathbf{u}^n\right)+\mathbf{G}^0 p^{n+1}=\mu\sum_{\alpha=1}^{3}G_\alpha^+G_\alpha^-\mathbf{u}^{n+1}+(\mathbf{f}^{\mathrm{b}})^n, \tag{57}$$

$$\mathbf{G}^0\cdot\mathbf{u}^{n+1}=0. \tag{58}$$

In these equations, the operator $\mathbf{G}^0 p$ approximates ∇p, and $\mathbf{G}^0\cdot\mathbf{u}$ approximates $\nabla\cdot\mathbf{u}$. In the viscous term, the expression $\sum_{\alpha=1}^{3}G_\alpha^+G_\alpha^-$ is a difference approximation to the Laplace operator. In the convection term, the expression $\sum_{\alpha=1}^{3}u_\alpha G_\alpha^{\pm}$, where

$$u_\alpha G_\alpha^{\pm}=\begin{cases}u_\alpha G_\alpha^+, & u_\alpha<0,\\ u_\alpha G_\alpha^-, & u_\alpha>0,\end{cases}$$

is an upwind difference approximation to $\mathbf{u}\cdot\nabla$. We use the FFT (fast Fourier transform) to solve the system (57)–(58). Note that this system is linear with constant coefficients in the unknowns $(\mathbf{u}^{n+1}, p^{n+1})$, the nonlinear terms being known since they are evaluated at time level n. The FFT therefore uncouples this system into N^3 separate 4×4 systems, which are easily solved.

Once $\mathbf{u}^{n+1}$ is known, the boundary points are moved at the locally averaged fluid velocity in this new velocity field. This is done as follows:

$$\frac{\mathbf{X}_k^{n+1}-\mathbf{X}_k^n}{\triangle t}=\sum_{\mathbf{x}}\mathbf{u}^{n+1}(\mathbf{x})\delta_c(\mathbf{x}-\mathbf{X}_k^n)h^3, \tag{59}$$

where $\sum_{\mathbf{x}}$ denotes the sum over the computational lattice $\mathbf{x}\in g_h$.

The last step of the numerical procedure is to update the orientation of the triad at each point s_k of the rod. Each such triad rotates at the local angular velocity of the fluid. Recall that the local angular velocity of a fluid element is $\frac{1}{2}\nabla\times\mathbf{u}$. We discretize this as $\frac{1}{2}\mathbf{G}^0\times\mathbf{u}$, and compute its local average at the point s_k of the rod as follows:

$$\mathbf{W}_k^{n+1}=\frac{1}{2}\sum_{\mathbf{x}\in g_h}(\mathbf{G}^0\times\mathbf{u}^{n+1})(\mathbf{x})\delta_c(\mathbf{x}-\mathbf{X}_k^n)h^3. \tag{60}$$

Now let $R(\mathbf{e},\theta)$ be the orthogonal matrix that describes a rotation through an angle θ about the axis specified by the unit vector $\mathbf{e}$. We can write R explicitly as follows:

$$R(\mathbf{e},\theta)=(\cos\theta)I+(1-\cos\theta)\mathbf{e}\mathbf{e}^T+(\sin\theta)(\mathbf{e}\times), \tag{61}$$

where $(\mathbf{e}\times)$ is the antisymmetric 3×3 matrix defined by $(\mathbf{e}\times)\mathbf{v}=\mathbf{e}\times\mathbf{v}$, for any $\mathbf{v}$. We emphasize that $\mathbf{e}$ is a unit vector. In terms of R, the rotation that we need to apply to the triad located at point s_k of the rod is given by

$$(\mathbf{D}_k^i)^{n+1}=R\left(\frac{\mathbf{W}_k^{n+1}}{|\mathbf{W}_k^{n+1}|},|\mathbf{W}_k^{n+1}|\triangle t\right)(\mathbf{D}_k^i)^n, \tag{62}$$

where $i=1,2,3$ and $k=0,\ldots,l-1$. Thus, we rotate each triad at the locally averaged angular velocity of the fluid for an amount of time equal to $\triangle t$, and this completes the time step.

Note that the above rotation is free in the sense that we do not constrain the vector $\mathbf{D}^3$ to be tangent to the curve that describes the axis of the rod. Insofar as $\mathbf{D}^3$ deviates from that direction, however, forces are called into play that tend to correct the misalignment. A similar remark may be made concerning the update of the position $\mathbf{X}(s)$. There is nothing in the updating procedure that constrains s to be arclength. Insofar as s deviates from arclength, however, forces develop that tend to correct for those deviations.

We conclude this section with a proof that the body force $\mathbf{f}^{\mathrm{b}}$ defined by (53) applies the correct total force and also the correct total torque to the fluid. To avoid complications associated with the definition of torque on a periodic domain, we imagine here the fluid domain is the whole three-dimensional Euclidean space and that g_h is an unbounded computational lattice. Since the rod is described by a continuous closed curve, it lives at any given time within a bounded subset of this domain. Because δ_c has bounded support, it is then clear that $\mathbf{f}^{\mathrm{b}}$ has bounded support as well. Thus, all of the sums that appear in the proof have only a finite number of nonzero terms, so there are no issues of convergence, and we do not have to worry about boundary terms when we do summation by parts. The proof given here relies in an essential way on the identities (37)–(38) stated in the previous section for δ_c, and the proof therefore requires the assumption that c/h is a positive integer.

First consider the total force applied by the rod to the fluid. We sum (53) over g_h and multiply by h^3. Now it is easy to see that

$$\sum_{\mathbf{x}\in g_h} (\mathbf{G}^0 \times \mathbf{v})(\mathbf{x}) h^3 = 0 \tag{63}$$

for any $\mathbf{v}(\mathbf{x})$ with bounded support, so the second term in $\mathbf{f}^{\mathrm{b}}$ makes no contribution. We are left with

$$\sum_{\mathbf{x}\in g_h} \mathbf{f}^{\mathrm{b}}(\mathbf{x}) h^3 = \sum_{k=0}^{l-1} (-\mathbf{f}_k) \sum_{\mathbf{x}\in g_h} \delta_c(\mathbf{x} - \mathbf{X}_k) h^3 \triangle s = \sum_{k=0}^{l-1} (-\mathbf{f}_k) \triangle s. \tag{64}$$

In the first step, we have interchanged the order to the two summations, and in the second step we have made use of (37).

Next we consider the more complicated case of the total torque. This time we apply the operator $\mathbf{x}\times$ to both sides of (53) before summing over $\mathbf{x} \in g_h$ and multiplying by h^3. We consider the two terms on the right-hand side separately. In analyzing the first term it is helpful to note that the two identities (37) and (38) can be combined to yield

$$\sum_{\mathbf{x}\in g_h} \mathbf{x} \delta_c(\mathbf{x} - \mathbf{X}) h^3 = \mathbf{X}. \tag{65}$$

Making use of this result, we see that

$$\begin{aligned} \sum_{\mathbf{x}\in g_h} \mathbf{x} \times \sum_{k=0}^{l-1} (-\mathbf{f}_k) \delta_c(\mathbf{x} - \mathbf{X}_k) \triangle s h^3 &= \sum_{k=0}^{l-1} \left(\sum_{\mathbf{x}\in g_h} \mathbf{x} \delta_c(\mathbf{x} - \mathbf{X}_k) h^3 \right) \times (-\mathbf{f}_k) \triangle s \\ &= \sum_{k=0}^{l-1} \mathbf{X}_k \times (-\mathbf{f}_k) \triangle s. \end{aligned} \tag{66}$$

In the case of the second term, it is helpful to work in components. The α component of the second term is

$$\frac{1}{2}\epsilon_{\alpha\beta\gamma}\epsilon_{\gamma\lambda\mu}\sum_{\mathbf{x}\in g_h} x^\beta G^0_\lambda \sum_{k=0}^{l-1}(-n_k^\mu)\delta_c(\mathbf{x}-\mathbf{X}_k)\triangle s h^3, \tag{67}$$

where we employ the summation convention and the totally antisymmetric symbol ϵ. This expression can be simplified by making use of summation by parts, in which we change the sign and apply G^0_λ to x^β instead of the expression on its right. It is easy to see that $G^0_\lambda x^\beta = \delta_{\lambda\beta}$. Now

$$\epsilon_{\alpha\beta\gamma}\epsilon_{\gamma\lambda\mu}\delta_{\beta\lambda} = (\delta_{\alpha\lambda}\delta_{\beta\mu} - \delta_{\alpha\mu}\delta_{\beta\lambda})\delta_{\beta\lambda} = (1-3)\delta_{\alpha\mu} = -2\delta_{\alpha\mu}. \tag{68}$$

It follows, with the help of the identity given by (37), that the expression given by (67) reduces all the way down to

$$\sum_{k=0}^{l-1}(-n_k^\alpha)\triangle s. \tag{69}$$

Combining this with the result for the first term, (66), we see that

$$\sum_{\mathbf{x}\in g_h}\mathbf{x}\times\mathbf{f}^{\mathrm{b}} = \sum_{k=0}^{l-1}((\mathbf{X}_k\times(-\mathbf{f}_k)) + (-\mathbf{n}_k))\triangle s. \tag{70}$$

Equations (64) and (70) show that our numerical algorithm does indeed apply the correct total force and the correct total torque to the fluid. These equations therefore imply that neither momentum nor angular momentum is spuriously created or destroyed in the rod-fluid interaction step of our computational scheme.

Because (64) and (70) are identities that hold for *any* distribution of force and torque applied by the rod to the fluid, and because the forces and torques are clearly applied *locally* on account of the bounded support of δ_c, the significance of these results is greater than it may at first appear. It is not merely a question of the *total* force and torque being correct, but also that the force and torque applied by any *part* of the rod are correctly transmitted to the fluid. This follows from the above by decomposing the force and torque into parts (e.g., by using a partition of unity along the rod), and then applying the above identities to each part separately.

5. Results and discussion. In this section, we study the evolution in time of a twisted ring immersed in a viscous incompressible fluid. The ring starts out in a configuration which is a perturbation of the circular equilibrium derived above (section 2). Depending on the parameters, the perturbation may decay, in which case the ring relaxes to the circular equilibrium configuration, or it may grow, in which case the ring and the surrounding fluid undergo a large-amplitude motion that eventually leads the ring into a stable coiled configuration in which self-contact of the ring plays an important role.

The computational and physical parameters that we regard as standard are summarized in Tables 1 and 2. Deviations from these values will be explicitly stated where they occur. A particularly important parameter is the number of twists, p, which we choose as an integer for reasons that have been discussed above. When other parameters are held fixed, the circular equilibrium of the ring is stable for sufficiently small

TABLE 1
Computational parameters.

Computational domain (cubic)	$10\,\text{cm} \times 10\,\text{cm} \times 10\,\text{cm}$
Fluid grid	$64 \times 64 \times 64$
Meshwidth for fluid, h	$0.1562\,\text{cm}$
Fluid density, ρ	1g/cm^3
Fluid viscosity, μ	$0.01\text{g/cm} \cdot \text{s}$
Radius of the unstressed rod, r_0	$2.5\,\text{cm}$
Number of boundary points, n_r	200
Meshwidth for rod, $\triangle s$	$0.0785\,\text{cm}$
Time step, $\triangle t$	$0.01\,\text{sec}$

TABLE 2
Material properties of the ring.

Bending modulus, $a_1 = a_2 = a$	$0.3\,\text{dyne} \cdot \text{cm}^2$
Twist modulus, a_3	$0.2\,\text{dyne} \cdot \text{cm}^2$
Shear force constant, $b_1 = b_2 = b$	$54\,\text{dyne}$
Stretch force constant, $b_3 = b$	$54\,\text{dyne}$
Number of twists, p	$0, 1, 2, 3, 4, 5, 6$

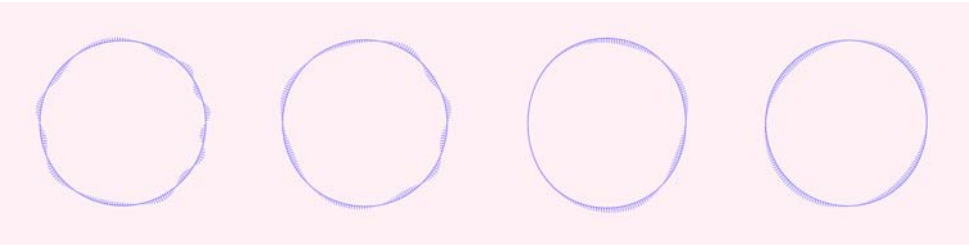

(a) $t = 0s$ (b) $t = 1.1s$ (c) $t = 2.5s$ (d) $t = 11s$

FIG. 3. (a) *Initial configuration with a ring (circle) and* $\mathbf{D}^1$*;* (b)–(d) *are snapshots at time* t *in seconds. Parameters: an intrinsic twist* $p = 2$*, elastic material properties* $a = 0.3$*,* $a_3 = \frac{2}{3}a$*,* $b = 54$ *in CGS (centimeter-gram-second) unit, and perturbation parameter* $\epsilon = 10$*.*

p and becomes unstable at some critical value of p. Also, in the unstable cases, the coiled configuration that the ring eventually finds depends on the value of p.

With these chosen parameters, we find that when $p = 0, 1, 2$, the circular equilibrium of the twisted ring is stable. When $p \geq 3$, the circular equilibrium is unstable, and the ring evolves into different coiled shapes that depend on p. In fact, as p increases, the number of loops in the final coiled configuration increases as well (see the second column of snapshots in Figure 7). Computational experiments show that a change in the value of the parameter b does not change the coiled equilibrium configurations for $1 < b \leq 300$.

Figure 3 shows motions at different instants when $p = 2$. The initial configuration in this case is a strong perturbation away from the circular equilibrium, since $\epsilon = 10$ (see (21)–(22)). Despite the large initial perturbation, we see that the ring relaxes back to the circular equilibrium in this case. (Compare Figure 3(d) and Figure 1(a).)

The writhing dynamics that emerge in cases $p = 4, 5, 7$, in which the circular equilibrium is unstable, are shown in Figures 4–6. In all three cases, we start very close to the circular equilibrium configuration by setting $\epsilon = 0.001$. Each figure shows the ring and its associated triad in blue, and selected fluid markers that start out

near the ring are shown in red. The fluid markers leave trails that show their recent trajectories. At each selected time, two different views of the ring and fluid markers are shown. The selected times are not equally spaced. Note in particular the long time that it takes the perturbation to grow to a significant size in comparison to the rapid evolution that happens thereafter. This is especially pronounced at the lower unstable values of p. Throughout the complicated motions shown in these figures, the ring retains its initial length to within 2%.

In Figure 4, the ring gradually takes on the configuration of a figure-eight structure (see frame (d)), and then the two loops of the figure-eight twist in opposite directions. The resulting coiled equilibrium is called a *plectoneme* [6, 13]. Note that the number of self-contact points increases with time as the ring approaches its coiled equilibrium.

Figure 5 shows the case in which the intrinsic twist is $p = 5$. The equilibrium configuration in Figure 5(e) has three points of self-contact and three loops. Figure 6 with $p = 7$ shows an equilibrium *clover* configuration with four self-contact points.

In Figure 7, we vary the twist modulus in order to see what impact that has on the stability of the ring. The figure shows an array of results after the motion has settled down. Each row corresponds to a particular value of the intrinsic twist p, and each column corresponds to a particular value of the twist modulus (reported in terms of the ratio of the twist modulus to the bend modulus, a_3/a). It is readily apparent from the figure that the stability boundary of the circular equilibrium configuration moves in the direction of lower intrinsic twist as the twist modulus increases. Another result of this study is that the number of loops formed during coiling increases both as a function of the intrinsic twist and also as a function of the twist modulus.

Note that the first and last columns of Figure 7 consider cases that cannot be achieved if the circular ring is made out of a homogeneous, isotropic elastic material with the whole cross section filled. We include these cases because the anisotropic microstructures that occur in biological settings make possible a wider range of ratios of the twist to the bend modulus.

When the circular equilibrium configuration is unstable, the coiled configuration that is eventually reached may depend on the initial condition. To study this, we compare results computed with all parameters held fixed other than ϵ, which measures the amplitude of the initial perturbation. Qualitatively different configurations of the ring appear, each associated with an interval of values of ϵ, as shown in Figure 8, which depicts a typical configuration for each such interval. In order of increasing ϵ, the configurations seen may be described as follows: (a) a three-leaf clover, (b) a configuration with two self-contact points, (c) a configuration with two well-separated *sets* of closely spaced contact points, and (d) a plectoneme. According to [6], the clover and plectoneme configurations are stable, but the others are not. This suggests that further evolution would have been seen in the two intermediate cases if we had waited long enough for it to occur.

In many of the above examples, the ring comes to rest in a configuration that involves self-contact. We emphasize that this occurs without any special mechanism for detecting or responding to a self-contact condition. Even though further reduction of the elastic potential energy would result from the ring moving through itself in these situations, it does not do so. In real life, self-crossing is prevented by the impenetrability of matter, or, as we sometimes say, by the reluctance of two things to be in the same place at the same time. This could be modeled by a high potential energy barrier. In the IB method, however, a different, more automatic, mechanism achieves the same end. Recall that, in the IB method, the immersed boundary moves

FIG. 4. *Snapshots showing the ring and all vectors of the triads at each boundary point at time t. Top row and bottom row illustrate side views and top views of the motion, respectively. The number of twists is* $p = 4$*, material properties are* $a = 0.3$*,* $a_3 = \frac{2}{3}a$*,* $b = 54$*, in CGS unit, and the perturbation parameter is* $\epsilon = 0.001$*. Fluid markers in red are spread around the ring and show their trajectories.*

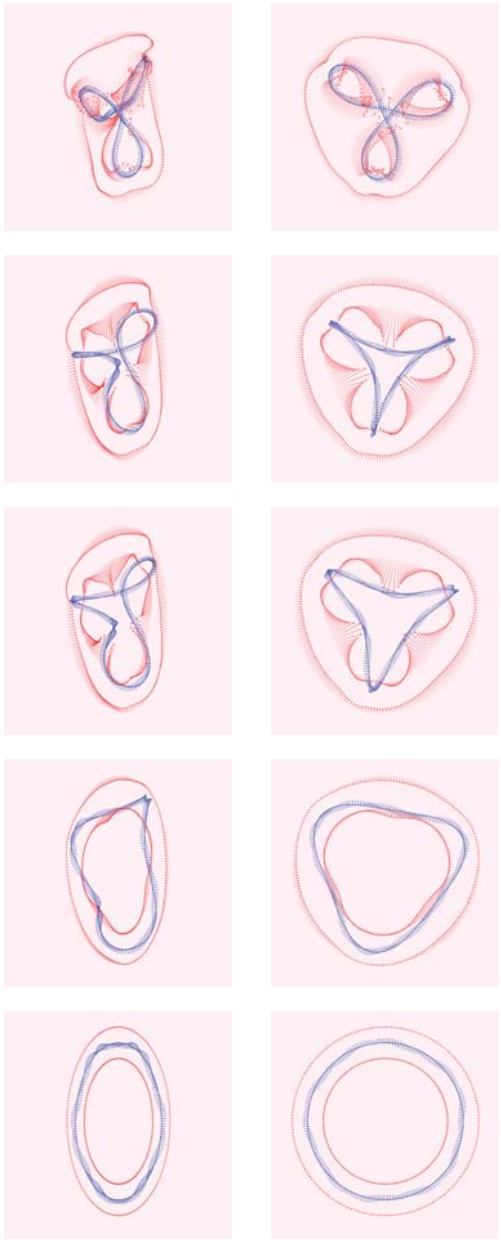

(a) $t = 0s$ (b) $t = 92s$ (c) $t = 97s$ (d) $t = 98s$ (e) $t = 105s$

FIG. 5. *Snapshots showing the ring and all vectors of the triads at each boundary point at time t together with fluid markers in red. Parameters: $p = 5$, $a = 0.3$, $a_3 = \frac{2}{3}a$, $b = 54$, and $\epsilon = 0.001$. The first row is viewed from the side and the second row from the top of the motion.*

FIG. 6. *Snapshots showing the ring and all vectors of the triads at each boundary point at time t together with fluid markers. Parameters: $p = 7$, $a = 0.3$, $a_3 = \frac{2}{3}a$, $b = 54$, and $\epsilon = 0.001$. The first row is viewed from the side and the second row from the top of the motion.*

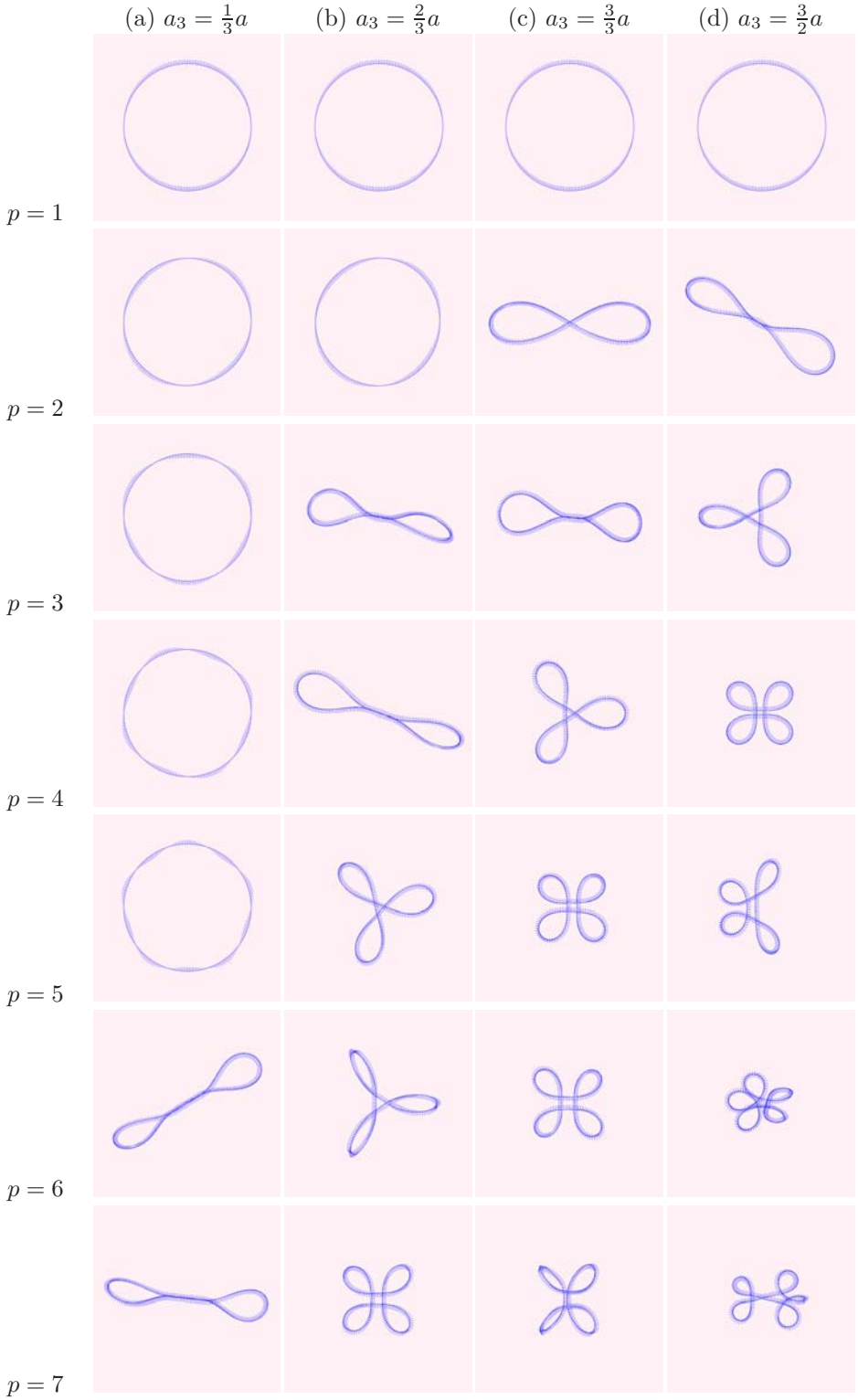

FIG. 7. *Collection of stable equilibria depending on ratio of* $\frac{a_3}{a}$ *and the initial twist* p. *Parameters:* $a = 0.3$, $b = 54$ *in CGS unit and* $\epsilon = 0.001$.

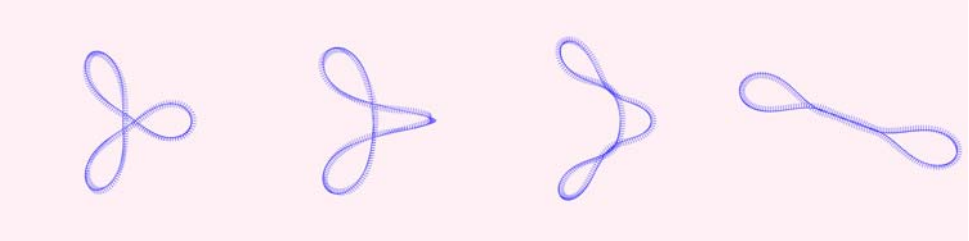

(a) $0 < \epsilon \leq 0.175$ (b) $0.2 \leq \epsilon \leq 0.275$ (c) $0.3 \leq \epsilon \leq 0.35$ (d) $\epsilon \geq 0.375$

FIG. 8. *Transition of configurations with the increments in perturbation parameter ϵ. All other parameters are fixed: $a = 0.3$, $a_3 = \frac{2}{3}a$, $b = 54$, and $p = 5$.*

in the continuous velocity field of the fluid. Therefore, at the level of the continuous formulation of the problem, self-crossing is impossible. Even after discretization, the IB points that represent the ring move in a continuous velocity field (with continuous first spatial derivatives) that is obtained by interpolation from the fluid grid. Nevertheless, self-crossing of the ring in the discrete case is possible, for two reasons: the continuous ring has been replaced by a discrete array of points, and the motion occurs in discrete time steps instead of continuously. In practice, though, when the time step is small enough, and when the spacing between the IB points is small enough in relation to the resolution of the fluid grid, self-crossing does not occur.

It is both amusing and instructive to see what happens when the numerical parameters are not well chosen, and self-crossing does occur (see Figure 9). First the immersed ring seems to settle into a coiled configuration with self-contact, like those shown above. It takes some time for self-crossing to occur, since the velocities of two IB points that are nearly in contact are nearly equal. Once self-crossing does occur, it reduces the number of twists in the ring, and this may change the stability of the circular equilibrium configuration from unstable to stable. In such a case, the ring that has crossed itself relaxes back to the circular configuration from which (except for a small perturbation) it started, although the final configuration is not really the same as the initial condition because of the reduction in the intrinsic twist that occurred during the topological transition in which the ring crossed itself.

In order to determine the empirical order of accuracy of the method, we compare numerical solutions obtained on four different meshes at a given time. As we refine the computational mesh of the fluid grid, we follow the unusual procedure of keeping the *physical* size of the support of the delta function constant. When we change from a 64^3 grid to a 128^3 grid, this implies that the numerical support of the delta function grows from 4^3 to 8^3 points. In physical variables, we use the same delta function in both cases; in units of meshwidths the delta function for the refined mesh is obtained from the one for the coarse mesh by a simple scaling by a factor of two in each space direction. The rationale for this procedure is that the diameter of the support of the delta function is a physical rather than a numerical parameter in this work; it corresponds at least roughly to the diameter of the rod, since it determines the size of the region of fluid with which any given point of the rod interacts directly, and therefore it should not be refined as the fluid grid is refined. (Recall that we represent the rod by an immersed space curve, together with an associated orthonormal triad at each point of that space curve. Such a curve, obviously, occupies zero volume, unlike the physical rod that we are trying to represent. There is, however, a nonzero volume of fluid within the support of the delta function, and this part of the fluid is the part

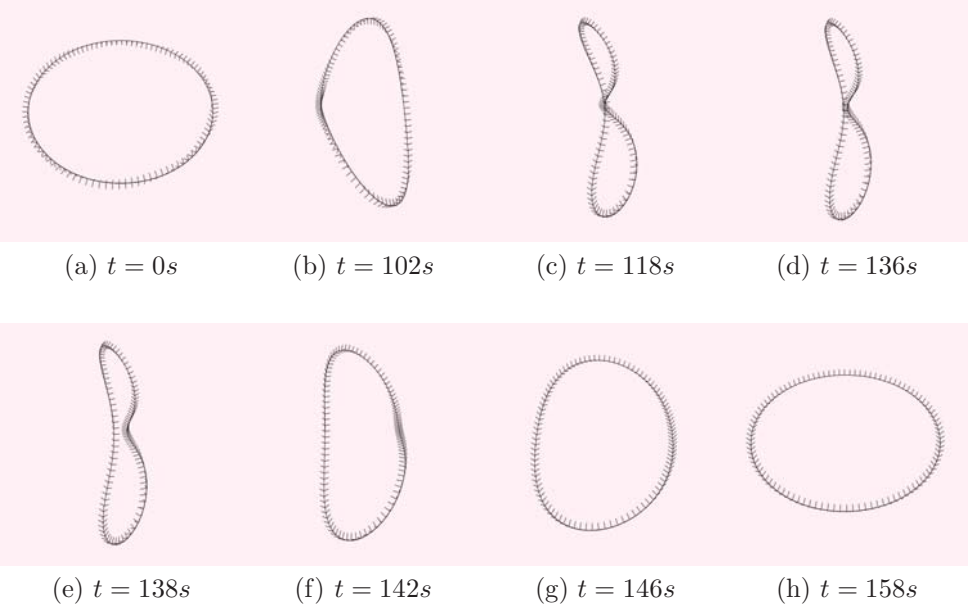

(a) $t = 0s$ (b) $t = 102s$ (c) $t = 118s$ (d) $t = 136s$

(e) $t = 138s$ (f) $t = 142s$ (g) $t = 146s$ (h) $t = 158s$

FIG. 9. *Self-crossing. The number of boundary points in this simulation is* $n_r = 100$*, which is too few to prevent self-crossing of the ring. Parameters:* $a = 0.3$, $a_3 = a$, $b = 54$, $\epsilon = 0.1$, $\triangle t = 0.01s$, $p = 2$. *Self-crossing occurs between frames* (c) *and* (d). *Note that the twist is reduced by this topological change. Close inspection of the triads in frame* (h) *shows that the twist has dropped to* $p = 0$.

that directly feels the force and torque generated by the rod, and also the part that directly determines the velocity with which the rod moves and the angular velocity with which its triads rotate. For these reasons, the volume of fluid within the support of the delta function in our IB formulation may be said to model the rod itself.)

To test the convergence of the method, we performed calculations for the same physical problem on four different grids, of sizes 32^3, 64^3, 128^3, and 256^3. The physical parameters of the problem were as follows: $a = 0.3$, $a_3 = 0.3$, $b = 54$, $p = 3$, and $\epsilon = 0.1$. This is a case in which the circular configuration is unstable, so the ring undergoes a large deformation from a near-circular configuration to a coiled configuration, and we first checked that the final coiled configuration was essentially the same in all four cases. Then, to assess convergence quantitatively, we compared the computed velocity fields at a particular time ($t = 40$s), which was chosen because that is the time at which the ring has evolved roughly halfway to its final configuration. In particular, this means that significant motion is still underway, so comparison of the velocity fields computed on different grids at this time is meaningful. The numerical parameters of the test are shown in Table 3. Note that the number of points n_r on the ring doubles, and also that the time step $\triangle t$ is halved, for each refinement of the meshwidth by a factor of two. Solutions computed on different grids are compared by evaluating the discrete L^2-norm of their difference (on those points that are common to the grids in question). Convergence ratios of these L^2-norm differences are displayed in Table 4. All of these ratios are close to 2, which indicates first order convergence.

6. Conclusion. In this paper, we have generalized the IB method so that it can be used to model an immersed elastic rod with bend and twist in a viscous incompressible fluid. In the original IB method, the immersed boundary interacts

TABLE 3
Parameter values for convergence study.

Grid size	n_r	$\triangle t$	δ_c
$32 \times 32 \times 32$	100	0.01s	2-point
$64 \times 64 \times 64$	200	0.005s	4-point
$128 \times 128 \times 128$	400	0.0025s	8-point
$256 \times 256 \times 256$	800	0.00125s	16-point

TABLE 4
Convergence ratios for velocity $\mathbf{u} = (u, v, w)$ *in* L^2*-norm.*

m	$\frac{\|\|u_m - u_{2m}\|\|_2}{\|\|u_{2m} - u_{4m}\|\|_2}$	$\frac{\|\|v_m - v_{2m}\|\|_2}{\|\|v_{2m} - v_{4m}\|\|_2}$	$\frac{\|\|w_m - w_{2m}\|\|_2}{\|\|w_{2m} - w_{4m}\|\|_2}$
32	2.2210	1.8568	2.0194
64	1.9599	1.9991	2.0937

with the fluid by moving at the local fluid velocity and applying force locally to the fluid. Here, the immersed boundary has an orientation as well as a position, the orientation being described by an orthonormal triad attached to each IB point. The new feature of the IB method described in this paper is that the interaction of the immersed boundary with the fluid now involves not only translation of the IB points at the local fluid velocity, but also rotation of the associated triads at the local fluid angular velocity. Similarly, we apply not only force but also torque to the fluid in which the bent twisted rod is immersed.

A key ingredient in the above scheme is a model of the bent twisted rod itself in which the triads that define the local orientation of the material are not strictly constrained to be aligned with the local tangent direction to the centerline of the rod. Instead, strong elastic forces are provided which tend to maintain such alignment without rigidly enforcing it. Similarly, we do not assume that arclength of a material segment of the rod is exactly constant, but we do provide strong elastic forces that oppose changes in the arclength of any material segment of the rod. Thus, our rod model generalizes that of Kirchhoff by replacing the constraints of the Kirchhoff rod model by penalty terms in the elastic energy that produce forces that tend to enforce those constraints. The formulation of this generalized Kirchhoff rod model is described in the appendix.

As an example application, we consider the motion in a viscous incompressible fluid of a bent twisted rod whose centerline takes the form of a closed space curve. As is well known, such a ring has an equilibrium configuration in which its centerline is a circle, with a uniform distribution of twist. Such an equilibrium may be stable or unstable. With all other parameters held constant, the equilibrium is stable for sufficiently small twist and becomes unstable when a critical value of the twist is reached. We have reproduced this phenomenology in the present paper, and, moreover, we have used the new IB method to study what happens to the ring and the surrounding fluid in the unstable case. Here, we observe various forms of supercoiling, in which the ring eventually comes to rest in a configuration that involves self-contact.

A particular strength of the IB method proposed here, and indeed of IB methods in general, is that the contact problem is solved in a completely effortless way. There is no need to test for contact or to do anything special about it. The fundamental reason for this is that the points that represent the immersed boundary move in an interpolated velocity field that is continuous (and, moreover, has continuous first derivatives) by construction. Thus, if we consider the idealized situation of an IB

method in which only the fluid grid is discretized, but the immersed boundary itself remains continuous, and in which time also remains continuous, then it is easy to see that two different immersed boundaries, or two parts of the same immersed boundary, cannot possibly cross, merely by continuity. In practice, of course, the immersed boundary is discretized and time proceeds in discrete steps, but if we take care to keep these two discretizations fine enough in relation to that of the fluid grid, then the contact problem is automatically solved. We see many instances of this in the supercoiling results of this paper, in which the bent twisted rod comes (nearly) to rest in configurations of (very near) self-contact. Indeed, it is striking in our computed results how closely the immersed boundary approaches itself without self-crossing.

We believe that the methods of this paper will find numerous applications in biological fluid dynamics. As an example, consider bacteria that swim by spinning long, thin, helical flagella. Such flagella are far from rigid. Indeed, when they all spin the same way they tend to wrap around each other, forming a "superflagellum" that propels the bacterium systematically in one direction [2]. Nevertheless, their elastic resistance to bend and twist is essential to their maintenance of a helical configuration, which in turn is essential for the development of thrust. With the original IB method, it was possible to model bacterial flagella only as three-dimensional structures immersed in fluid [20]. The methods of the present paper make it possible to model bacterial flagella in a one-dimensional manner: as immersed space curves with a triad (material frame) at each point. The extreme thinness of bacterial flagella in relation to their length suggests that this is their more natural representation.

Appendix. The unconstrained Kirchhoff rod model. We sketch here the derivation of the equilibrium equations of the unconstrained Kirchhoff rod model that is used in this paper. The state of the rod is described by a space curve $\mathbf{X}(s)$ and an associated orthonormal triad at each s, $\{\mathbf{D}^1(s), \mathbf{D}^2(s), \mathbf{D}^3(s)\}$, $0 \le s \le L$, where L is the unstressed length of the rod. We assume that the rod is closed on itself, forming a loop, and that $\mathbf{X}(s), \mathbf{D}^1(s), \mathbf{D}^2(s), \mathbf{D}^3(s)$ are all smoothly periodic with period L. The rod is subject to applied forces and couples denoted $\mathbf{f}(s)ds$ and $\mathbf{n}(s)ds$, respectively. The internal forces and couples transmitted across a section of the rod at s are denoted $\mathbf{F}(s)$ and $\mathbf{N}(s)$, respectively, with the sign convention that these are the forces and couples applied by the part of the rod with $s' > s$ near s to the part of the rod with $s' < s$ near s across the section of the rod at s.

Because $\{\mathbf{D}^1(s), \mathbf{D}^2(s), \mathbf{D}^3(s)\}$ is an orthonormal triad, we have the constraints

$$\mathbf{D}^i(s) \cdot \mathbf{D}^j(s) = \delta_{ij} \tag{71}$$

which we impose exactly. The sense in which our Kirchhoff rod model is unconstrained is that we do not require $\mathbf{D}^3$ to be aligned with the tangent vector to the axis of the rod $\partial\mathbf{X}/\partial s$, nor do we assume that $|\partial\mathbf{X}/\partial s| = 1$. Instead, we provide an energy penalty for deviations from these conditions, so that they tend to be maintained approximately instead of exactly. One advantage of this penalty approach is that we thereby obtain an explicit formula for the force $\mathbf{F}(s)$ that is transmitted across each section of the rod in terms of the configuration of the rod and its triad. Another advantage of the penalty formulation is that we thereby avoid imposing complicated constraints on the fluid motion in the neighborhood of the rod.

Because the transport of the triad along the rod is that of a rigid body, there must be a vector field $\mathbf{K}(s)$ such that

$$\frac{\partial \mathbf{D}^i}{\partial s} = \mathbf{K} \times \mathbf{D}^i. \tag{72}$$

The components of $\mathbf{K}$ in the basis $\{\mathbf{D}^1, \mathbf{D}^2, \mathbf{D}^3\}$ are known as the *curvatures* of the rod, and a fundamental assumption of Kirchhoff rod theory is that

$$N_k(s) = a_k K_k(s) \tag{73}$$

for $k = 1, 2, 3$, where the N_k are the components of $\mathbf{N}$ in the basis $\{\mathbf{D}^1, \mathbf{D}^2, \mathbf{D}^3\}$. We assume here that the rod is homogeneous, so that the a_k do not depend on s, and, moreover, we assume that the triad has been set up in the *relaxed* configuration of the rod in such a way that $\mathbf{D}^1$ and $\mathbf{D}^2$ are perpendicular to the axis of the rod and aligned with the principal axes of the cross section. The constants a_1 and a_2 are called bending moduli, and the constant a_3 is the twisting modulus of the rod.

The equations of equilibrium can be derived in two ways, and comparison of the two results is very instructive. The first method is to consider force and torque balance for an arbitrary interval of the rod, say (s_1, s_2). These considerations give

$$0 = \int_{s_1}^{s_2} \mathbf{f}(s) ds + \mathbf{F}(s)\big|_{s_1}^{s_2}, \tag{74}$$

$$0 = \int_{s_1}^{s_2} \left(\mathbf{n}(s) + (\mathbf{X}(s) \times \mathbf{f}(s))\right) ds + \left(\mathbf{N}(s) + (\mathbf{X}(s) \times \mathbf{F}(s))\right)\big|_{s_1}^{s_2}. \tag{75}$$

In (74), we use the fundamental theorem of calculus to combine the two terms:

$$0 = \int_{s_1}^{s_2} \left(\mathbf{f} + \frac{\partial \mathbf{F}}{\partial s}\right) ds. \tag{76}$$

Then, since s_1 and s_2 are arbitrary,

$$0 = \mathbf{f} + \frac{\partial \mathbf{F}}{\partial s}. \tag{77}$$

Equation (75) can be manipulated in a similar way, and the result can be simplified with the help of (77). When this is done, we get

$$0 = \mathbf{n} + \frac{\partial \mathbf{N}}{\partial s} + \left(\frac{\partial \mathbf{X}}{\partial s} \times \mathbf{F}\right). \tag{78}$$

Equations (77)–(78) are the equilibrium equations in vector form. They implicitly involve the triad configuration $\{\mathbf{D}^1(s), \mathbf{D}^2(s), \mathbf{D}^3(s)\}$ through (72) and (73).

In the standard Kirchhoff rod theory, these equations are supplemented by the constraint $\partial \mathbf{X}/\partial s = \mathbf{D}^3$, which states that $\mathbf{D}^3$ is tangent to the axis of the rod, and, moreover, since $\mathbf{D}^3$ is a unit vector, that $s =$ arclength. We avoid this constraint here and use a penalty formulation instead. This brings us to the second derivation of the equilibrium equations.

We assume that the elastic energy of the rod is given by

$$E = \frac{1}{2} \int_0^L \sum_{i=1}^{3} \left(a_i K_i^2 + b_i \left(\frac{\partial \mathbf{X}}{\partial s} \cdot \mathbf{D}^i - \delta_{3i}\right)^2\right) ds, \tag{79}$$

where the a_i have the same meaning as before, and where the new parameters b_i are the penalty constants. The parameters b_1 and b_2 may be interpreted as shear moduli, and b_3 is an extension modulus. The theory we derive here reduces to the standard theory as $b_i \to \infty$ for $i = 1, 2, 3$.

We may eliminate the K_i from (79) by solving (72) for K_i. To do this, let (i,j,k) be any cyclic permutation of $(1,2,3)$, and write (72) in terms of j instead of i:

$$\frac{\partial \mathbf{D}^j}{\partial s} = \mathbf{K} \times \mathbf{D}^j. \tag{80}$$

Then take the dot product of both sides with $\mathbf{D}^k$:

$$\frac{\partial \mathbf{D}^j}{\partial s} \cdot \mathbf{D}^k = \left(\mathbf{K} \times \mathbf{D}^j\right) \cdot \mathbf{D}^k = \mathbf{K} \cdot \left(\mathbf{D}^j \times \mathbf{D}^k\right) = \mathbf{K} \cdot \mathbf{D}^i = K_i. \tag{81}$$

Thus, the elastic energy may be expressed entirely in terms of $\mathbf{X}(s), \mathbf{D}^1(s), \mathbf{D}^2(s), \mathbf{D}^3(s)$, as follows:

$$E = \frac{1}{2} \int_0^L \sum_{i=1}^{3} \left(a_i \left(\frac{\partial \mathbf{D}^j}{\partial s} \cdot \mathbf{D}^k \right)^2 + b_i \left(\frac{\partial \mathbf{X}}{\partial s} \cdot \mathbf{D}^i - \delta_{3i} \right)^2 \right) ds. \tag{82}$$

Here, and throughout this appendix, (i,j,k) always denotes a cyclic permutation of $(1,2,3)$.

To find the equations of equilibrium of the rod under applied forces and couples, we invoke the principle of virtual work. The work done on the rod, to first order, by the applied forces $\mathbf{f}(s)ds$ and by the applied couples $\mathbf{n}(s)ds$, during a virtual displacement $\mathbf{X} \to \mathbf{X} + \delta\mathbf{X}$ and a virtual rotation of the triad $\mathbf{D}^i \to \mathbf{D}^i + \delta\mathbf{D}^i$, where

$$\delta \mathbf{D}^i = \delta \boldsymbol{\Omega} \times \mathbf{D}^i, \tag{83}$$

is given by

$$\delta \mathcal{W} = \int_0^L \left(\mathbf{f} \cdot \delta \mathbf{X} + \mathbf{n} \cdot \delta \boldsymbol{\Omega} \right) ds. \tag{84}$$

As we did previously with $\mathbf{K}$, we can find the components of $\delta\boldsymbol{\Omega}$ in the basis $\{\mathbf{D}^1, \mathbf{D}^2, \mathbf{D}^3\}$ from (83). The result is

$$\delta \mathbf{D}^j \cdot \mathbf{D}^k = \delta \Omega_i. \tag{85}$$

Thus (84) may be rewritten as follows:

$$\delta \mathcal{W} = \int_0^L \left(\mathbf{f} \cdot \delta \mathbf{X} + \sum_{i=1}^{3} n_i \delta \mathbf{D}^j \cdot \mathbf{D}^k \right) ds. \tag{86}$$

We are now ready to apply the principle of virtual work, with Lagrange multipliers to enforce the constraints $\mathbf{D}^i \cdot \mathbf{D}^j = \delta_{ij}$. We note that these constraints are of two types ($i \neq j$ and $i = j$), with three of each type. Accordingly, we introduce the constraint function

$$E_{\mathrm{c}} = \int_0^L \sum_{i=1}^{3} \left(q_i \mathbf{D}^j \cdot \mathbf{D}^k + r_i \left(\mathbf{D}^i \cdot \mathbf{D}^i - 1 \right) \right) ds, \tag{87}$$

where $q_i(s)$ and $r_i(s)$ are the six Lagrange multiplier functions. Note that $E_{\mathrm{c}} = 0$ for arbitrary $q_i(s)$ and $r_i(s)$ if and only if the constraints $\mathbf{D}^i \cdot \mathbf{D}^j = \delta_{ij}$ are satisfied.

The principle of virtual work with Lagrange multipliers now takes the following form:

$$\delta \mathcal{W} = \delta E + \delta E_{\mathrm{c}} \tag{88}$$

for arbitrary $\delta \mathbf{X}(s), \delta \mathbf{D}^1(s), \delta \mathbf{D}^2(s), \delta \mathbf{D}^3(s)$ that are smoothly periodic. We leave it as a (lengthy!) exercise for the reader to show, after eliminating the Lagrange multipliers, that the principle of virtual work implies the following two equations of equilibrium:

$$0 = \mathbf{f} + \frac{\partial \mathbf{F}}{\partial s}, \tag{89}$$

$$0 = n_i + a_i \frac{\partial K_i}{\partial s} + (a_k - a_j) K_j K_k + (F_k \mathbf{D}^j - F_j \mathbf{D}^k) \cdot \frac{\partial \mathbf{X}}{\partial s}, \tag{90}$$

where we have made the definitions

$$F_i = b_i \left(\frac{\partial \mathbf{X}}{\partial s} \cdot \mathbf{D}^i - \delta_{3i} \right), \tag{91}$$

$$\mathbf{F} = \sum_{i=1}^{3} F_i \mathbf{D}^i. \tag{92}$$

Equation (89) already agrees with the first of our equilibrium equations (77), but now we have an explicit formula for $\mathbf{F}$, (91)–(92), which we did not have before. This is the main benefit of the penalty formulation.

It remains only to compare (90) with the second equilibrium equation, (78). To do so, we note the following identities, which may be verified by the reader:

$$a_i \frac{\partial K_i}{\partial s} + (a_k - a_j) K_j K_k = \frac{\partial \mathbf{N}}{\partial s} \cdot \mathbf{D}^i, \tag{93}$$

$$\frac{\partial \mathbf{X}}{\partial s} \cdot \left(F_k \mathbf{D}^j - F_j \mathbf{D}^k \right) = \left(\frac{\partial \mathbf{X}}{\partial s} \times \mathbf{F} \right) \cdot \mathbf{D}^i. \tag{94}$$

Thus, (90) is the i component of the vector equation

$$0 = \mathbf{n} + \frac{\partial \mathbf{N}}{\partial s} + \left(\frac{\partial \mathbf{X}}{\partial s} \times \mathbf{F} \right), \tag{95}$$

which agrees perfectly with the second equilibrium equation, (78).

Thus, we have reached the possibly surprising conclusion that the vector form of the equations of equilibrium of our unconstrained Kirchhoff rod model are *exactly* the same as the vector equations of equilibrium of the standard Kirchhoff rod, with the only difference being that in the unconstrained case we get an explicit formula for $\mathbf{F}$ to replace the missing constraint equation $\partial \mathbf{X}/\partial s = \mathbf{D}^3$.

It should be noted, however, that the two sets of equations are *not* exactly the same when resolved into components in the basis $\{\mathbf{D}^1, \mathbf{D}^2, \mathbf{D}^3\}$. This is because that basis is itself slightly rotated in the unconstrained case in comparison to its configuration in the constrained case. It turns out that the first equilibrium equation is exactly the same in the two cases despite this rotation. To see what happens to the second equilibrium equation, though, we note that (91) can be rewritten as

$$\frac{\partial \mathbf{X}}{\partial s} \cdot \mathbf{D}^i = \delta_{3i} + \frac{F_i}{b_i}, \tag{96}$$

and that this allows us to rewrite (90) as follows:

$$0 = n_i + a_i \frac{\partial K_i}{\partial s} + (a_k - a_j) K_j K_k + (F_k \delta_{3j} - F_j \delta_{3k}) + F_j F_k \left(\frac{1}{b_j} - \frac{1}{b_k} \right) \tag{97}$$

for $i = 1, 2, 3$, with (i, j, k) a cyclic permutation of $(1, 2, 3)$ in each case. Since the standard Kirchhoff rod model is obtained from our unconstrained rod model by letting all of the $b_i \to \infty$, we see that (97) differs from the corresponding equation in the standard case only by virtue of the last term, and, moreover, we see that this term can be made to vanish, not only by letting all of the b_i approach infinity, but alternatively by setting all of the b_i equal to each other, as we have done in the present work.

Acknowledgments. Our code for the simulation of the bent twisted rod immersed in fluid is built upon IB software by Nathaniel Cowen, David McQueen, and C. S. Peskin. We are indebted to David McQueen and Estarose Wolfson for the use of their visualization software and also for their technical assistance. We thank Yongsam Kim and David Swigon for useful discussions.

REFERENCES

[1] S. S. Antman, *Nonlinear Problems of Elasticity*, Springer-Verlag, New York, 1995.
[2] H. C. Berg, *The rotary motor of bacterial flagella*, Annu. Rev. Biochem., 72 (2003), pp. 19–54.
[3] T. C. Bishop, R. Cortez, and O. O. Zhmudsky, *Investigation of bend and shear waves in a geometrically exact elastic rod model*, J. Comput. Phys., 193 (2004), pp. 642–665.
[4] B. D. Coleman and D. Swigon, *Supercoiled configurations with self-contact in the theory of the elastic rod model for DNA plasmids*, J. Elasticity, 60 (2000), pp. 171–221.
[5] B. D. Coleman and D. Swigon, *Theory of self-contact in Kirchhoff rods with applications to supercoiling of knotted and unknotted DNA plasmids*, Philos. Trans. R. Soc. Lond. Ser. A Math. Phys. Eng. Sci., 362 (2004), pp. 1281–1299.
[6] B. D. Coleman, D. Swigon, and I. Tobias, *Elastic stability of DNA configurations.* II. *Supercoiled plasmids with self-contact*, Phys. Rev. E (3), 61 (2000), pp. 759-770.
[7] E. H. Dill, *Kirchhoff's theory of rods*, Arch. Hist. Exact Sci., 44 (1992), pp. 2–23.
[8] R. Dillon, L. Fauci, and D. Gaver, III, *A microscale model of bacterial swimming, chemotaxis and substrate transport*, J. Theoret. Biol., 177 (1995), pp. 325–340.
[9] L. Fauci and C. S. Peskin, *A computational model of aquatic animal locomotion*, J. Comput. Phys., 77 (1988), pp. 85–108.
[10] A. Ferent, C. S. Peskin, and X. Wang, *Modeling a bent twisted filament immersed in fluid*, in Proceedings of the 7th U.S. National Congress on Computational Mechanics, Albuquerque, NM, 2003.
[11] A. L. Fogelson, *A mathematical model and numerical method for studying platelet adhesion and aggregation during blood clotting*, J. Comput. Phys., 56 (1984), pp 111–134.
[12] E. Givelberg, *Modelling elastic shells immersed in fluid*, Comm. Pure Appl. Math., 57 (2004), pp. 283–309.
[13] R. E. Goldstein, T. R. Powers, and C. H. Wiggins, *Viscous nonlinear dynamics of twist and writhe*, Phys. Rev. Lett., 80 (1998), pp. 5232–5235.
[14] A. Goriely and M. Tabor, *Nonlinear dynamics of filaments* I. *Dynamical instabilities*, Phys. D, 105 (1997), pp. 20–44.
[15] A. Goriely and M. Tabor, *Nonlinear dynamics of filaments* II. *Nonlinear analysis*, Phys. D, 105 (1997), pp. 45–61.
[16] A. Goriely and M. Tabor, *The nonlinear dynamics of filaments*, Nonlinear Dynam., 21 (2000), pp. 101–133.
[17] K. A. Hoffman, R. S. Manning, and J. H. Maddocks, *Link, twist, energy, and the stability of DNA minicircles*, Biopolymers, 70 (2003), pp. 145–157.
[18] E. Jung and C. S. Peskin, *Two-dimensional simulations of valveless pumping using the immersed boundary method*, SIAM J. Sci. Comput., 23 (2001), pp. 19–45.
[19] I. Klapper, *Biological applications of the dynamics of twisted elastic rods*, J. Comput. Phys., 125 (1996), pp. 325–337.
[20] S. Lim and C. S. Peskin, *Simulations of the whirling instability by the immersed boundary method*, SIAM J. Sci. Comput., 25 (2004), pp. 2066–2083.

[21] A. E. Love, *A Treatise on the Mathematical Theory of Elasticity*, Cambridge University Press, Cambridge, UK, 1892.
[22] N. H. Mendelson, *Helical growth of Bacillus subtilis: A new model of cell growth*, Proc. Natl. Acad. Sci. USA, 73 (1976), pp. 1740–1744.
[23] N. H. Mendelson, *Bacterial growth and division: Genes, structures, forces and clocks*, Microbiol. Rev., 46 (1982), pp. 341–375.
[24] N. H. Mendelson, J. J. Thwaites, J. O. Kessler, and C. Li, *Mechanics of bacterial macrofiber initiation*, J. Bacteriol., 177 (1995), pp. 7060–7069.
[25] C. S. Peskin, *Flow patterns around heart valves: A numerical method*, J. Comput. Phys., 10 (1972), pp. 252–271.
[26] C. S. Peskin, *Numerical analysis of blood flow in the heart*, J. Comput. Phys., 25 (1977), pp. 220–252.
[27] C. S. Peskin, *The immersed boundary method*, Acta Numer., 11 (2002), pp. 479–517.
[28] C. S. Peskin and D. M. McQueen, *Fluid dynamics of the heart and its valves*, in Case Studies in Mathematical Modeling: Ecology, Physiology, and Cell Biology, H. G. Othmer, F. R. Adler, M. A. Lewis, and J. C. Dallon, eds., Prentice–Hall, Englewood Cliffs, NJ, 1996, pp. 309–337.
[29] T. Schlick, *Modeling superhelical DNA: Recent analytical and dynamic approaches*, Curr. Opin. Struct. Biol., 5 (1995), pp. 245–262.
[30] T. Schlick and W. K. Olson, *Trefoil knotting revealed by molecular dynamics simulations of supercoiled DNA*, Science, 257 (1992), pp. 1110–1115.
[31] T. R. Strick, J. F. Allemand, D. Bensimon, and V. Croquette, *Behavior of supercoiled DNA*, Biophys. J., 74 (1998), pp. 2016–2028.
[32] C. W. Wolgemuth, R. E. Goldstein, and T. R. Powers, *Dynamic supercoiling bifurcations of growing elastic filaments*, Phys. D, 190 (2004), pp. 266–289.
[33] Y. Yang, I. Tobias, and W. K. Olson, *Finite element analysis of DNA supercoiling*, J. Chem. Phys., 98 (1993), pp. 1673–1686.
[34] L. Zhu and C. S. Peskin, *Simulation of a flapping flexible filament in a flowing soap film by the immersed boundary method*, J. Comput. Phys., 179 (2002), pp. 452–468.